https://doi.org/10.5194/acp-2021-725
Preprint. Discussion started: 3 September 2021
© Author(s) 2021. CC BY 4.0 License.

Atmospheric Chemistry and Physics Discussions

Development and application of a street-level meteorology and pollutant tracking system (S-TRACK)

Huan Zhang[1,2], Sunling Gong[1]*, Lei Zhang[1]*, Jianjun He[1], Yaqiang Wang[1], Lixin Shi[2,3], Jingyue Mo[1], Huabing Ke[1], Shuhua Lu[1]

[1] State Key Laboratory of Severe Weather & Key Laboratory of Atmospheric Chemistry of CMA, Chinese Academy of Meteorological Sciences, Beijing 100081, China
[2] Key Laboratory of Meteorology and Ecological Environment of Hebei Province, Shijiazhuang 050000, China
[3] Meteorological Institute of Hebei Province, Shijiazhuang 050000, China

Correspondence to: Sunling Gong (gongsl@cma.gov.cn) and Lei Zhang (leiz09@cma.gov.cn)

Abstract. A multi-model simulation system for street level circulation and pollutant tracking (S-TRACK) has been developed by integrating the Weather Research and Forecasting (WRF), the Computational Fluid Dynamics (CFD) and the Flexible Particle (FLEXPART) models. The winter wind environmental characteristics and the potential impact of a traffic source on nearby sites (about 300 to 400 m) in Jinshui district of Zhengzhou, China are analyzed with the system. It is found that the existence of buildings complicates the structure of the wind fields. The wind speed inside the building block is smaller than the background wind speed due to the dragging effect of dense buildings. Ventilation is better when the dominant airflow is in the same direction as the building layout. Influenced by the building layout, local circulations show that the windward side of the building is mostly the divergence zone and the leeward side is mostly the convergence zone, which is more obvious for high buildings and influencing

https://doi.org/10.5194/acp-2021-725
Preprint. Discussion started: 3 September 2021
© Author(s) 2021. CC BY 4.0 License.

Atmospheric Chemistry and Physics Discussions

air pollution transport at the street-level. Using the traffic source (line source) on a road within a city block, the system was applied to investigate the potential impact of a line source on specific sites under the influence of the streel-level circulations. The potential contribution ratio was estimated by the method of residence time analysis and to a particular site found to vary with the height of the site with a peak not at the ground but on a certain height. The results of the study are helpful to understand the characteristics of wind environment and effect of traffic emissions in the area, which is important to improve urban living environment and control air pollution.

1. Introduction

In recent decades, with the continuous development of urban construction in China, urban environmental problems have become increasingly serious and attracted widespread attentions. According to the 2019 China Ecological Environment Status Bulletin, 180 of 337 cities at the prefecture level exceeded ambient air quality standards. The complex building layouts and differences in thermal structures within cities lead to extremely complicated meteorological characteristics and pollutant transport in urban areas (Lei et al., 2012; Fernando et al., 2010; Aynsley, 1989). Though the diffusion of

https://doi.org/10.5194/acp-2021-725
Preprint. Discussion started: 3 September 2021
© Author(s) 2021. CC BY 4.0 License.

Atmospheric Chemistry and Physics Discussions

atmospheric pollution in urban areas is widely studied, the study on tracking the sources of pollutants on the street-level is still lacking due to limitations in research methods.

The research on the street-level atmospheric environment is mainly divided into three methods: field measurements (Macdonald et al., 1997), laboratory simulation research (Mavroidis et al., 2003), and model simulations (W. et al., 2015; Yucong et al., 2014; Hendricks et al., 2007). The model simulation has become one of the main methods for studying environmental problems at the street-level due to the easy control of simulation conditions and simple processing steps. The Computational Fluid Dynamics (CFD) is a numerical simulation method to study fluid thermal-dynamic problems and is now widely used in the studies related to microscale problems within the urban canopy (Gosman, 1999). The core of CFD simulation method is to solve the Navier-Stokes equations. Depending on the turbulence closure scheme, CFD pre-processing models can be divided into three types: Direct numerical simulation (DNS), Reynolds-averaged Navier–Stokes (RANS) (Liu et al., 2018; Zheng et al., 2015; Milliez and Carissimo, 2008) and Large eddy simulation (LES) (Kurppa et al., 2018; Li et al., 2008; Sada and Sato, 2002). The choice among the three methods depends on the costs and objectives. One of the most important issues in using CFD technology to research atmospheric environment problems on the street-level is to obtain accurate initial and

https://doi.org/10.5194/acp-2021-725
Preprint. Discussion started: 3 September 2021
© Author(s) 2021. CC BY 4.0 License.

Atmospheric Chemistry and Physics Discussions

boundary conditions (Ehrhard et al., 2000). To solve this problem, the multi-scale coupling method is revealed as a good solution, which uses the meteorological information from mesoscale model as the initial and boundary conditions to drive CFD (Nelson et al., 2016). Tewari et al. (2010) proved that the CFD simulation was improved significantly when the results of Weather Research and Forecasting (WRF) model were used as the initial and boundary conditions. With the WRF model, the community multiscale air quality (CMAQ) model, and the CFD (RANS) approach, Kwak et al. (2015) built an urban air quality modeling system, which shown better performance than the WRF-CMAQ model in simulating NO_2 and O_3 concentrations.

There is still a lack of research on pollutant sources in the study of street-level air pollution transport. The Flexible Particle (FLEXPART) model (Stohl et al., 2005; Stohl, 2003) is a gas-block trajectory-particle diffusion model based on the Lagrangian particle method. Initially, the FLEXPART model was driven by global meteorological reanalysis data from ECMWF or NCEP. In 2006,Fast and Easter (2006) combined the WRF and the FLEXPART model together and optimized when it came to technical level and output results. Nowadays, the WRF-FLEXPART model has been widely used to research the regional transport of air pollutants (Yu et al., 2020; He et al., 2020; Gao et al., 2020; He et al., 2017a; Brioude et al., 2013; De Foy et al., 2011). The FLEXPART model can

https://doi.org/10.5194/acp-2021-725
Preprint. Discussion started: 3 September 2021
© Author(s) 2021. CC BY 4.0 License.

Atmospheric Chemistry and Physics Discussions

track the transport and diffusion of tracers via forward or backward simulation. Different from Euler's model, the spatial resolution is not affected by the numerical dispersion in the integration process and can be maintained with high accuracy during the simulation. Therefore, it is suitable to apply FLEXPART model to trace the source of street-level air pollution. Cécé et al. (2016) firstly applied the FLEXPART model at a small-scale resolution to analyze potential sources of NO_X in urban areas, with the WRF-LES model results as the driving field. Though FLEXPART has been extensively applied in medium and long-range transport cases (Madala et al., 2015; Heo et al., 2015; Sandeepan et al., 2013; Liu et al., 2013), it has been rarely tested for street-level transport and small-scale resolution grids.

In this study, a multi-model simulation system for street level circulation and pollutant tracking (S-TRACK) was developed by integrating the WRF mesoscale, the CFD street scale and the FLEXPART particle diffusion models, to study the flow field characteristics and potential impact of traffic pollution to receptor sites, under real building scenarios and atmospheric conditions.

https://doi.org/10.5194/acp-2021-725
Preprint. Discussion started: 3 September 2021
© Author(s) 2021. CC BY 4.0 License.

Atmospheric Chemistry and Physics Discussions

2. Data and Methods

2.1 S-TRACK description

The S-TRACK system consists of three major components (Fig. 1). The WRF model is used to obtain the mesoscale three dimensions (3D) meteorological data, with the initial and boundary conditions provided by NCEP reanalysis data. The CFD model is used to obtain refined 3D street-level wind field data with a resolution of 1 m to 100 m in the simulation area, with the initial and boundary meteorological conditions provided by the WRF simulations. The FLEXPART model is coupled to analyze the street-level sources of atmospheric pollution transports, with driving wind field data from the CFD simulations and other meteorological data from the WRF simulations.

2.2 WRF model configuration

The WRF-ARW model (version 4.1.2) is used to simulate meteorological fields on the urban scale, and the results are used as the initial and boundary conditions to drive the CFD model. In this study, the WRF model is configured with four nested domains (Fig. 2a), with the resolution of 27 km × 27 km (85 × 85 grids), 9 km × 9 km (82 × 82 grids), 3 km × 3 km (82 × 82 grids), and 1 km × 1 km (61 × 61 grids), respectively. Vertically, there are 45 full eta levels from the surface to 100 hPa with 11 levels below 2

https://doi.org/10.5194/acp-2021-725
Preprint. Discussion started: 3 September 2021
© Author(s) 2021. CC BY 4.0 License.

Atmospheric Chemistry and Physics Discussions

km, on which the meteorological fields are used to drive the CFD model. The innermost nested region is shown in Fig. 2b, where the area focused in this study is marked with black box. The initial and boundary conditions of WRF model are obtained from the NCEP re-analysis data (http://rda.ucar.edu/dataset-s/ds083.2). The boundary conditions are updated every 6 hr. Table 1 lists the selected physical parameterization schemes. The time from 12:00 Beijing time (BJT) on December 30, 2018 to 23:00 BJT on January 31, 2019 is chosen as the modeling period, with the simulation results recorded once per hour.

2.3 CFD configuration

The STAR-CCM+, one of the most commonly used commercial CFD software, was selected for the street-level simulation. The model has powerful functions such as geometric modeling, model pre-processing, the calculation execution, and post-processing of results. It has advantages in meshing and has the ability to analyze fluid flow. More details on STAR-CCM+ can be found at https://www.plm.automation.siemens.com/global/zh/products/simcenter/STAR-CCM.html.

https://doi.org/10.5194/acp-2021-725
Preprint. Discussion started: 3 September 2021
© Author(s) 2021. CC BY 4.0 License.

Atmospheric Chemistry and Physics Discussions

2.3.1 3D street-level model construction and grid setting

The establishment of a 3D geometric model is based on the actual terrain and buildings data of the simulated area, which is obtained through drone aerial photography technology. In the process of model construction, the same shape as the actual building was maintained to reduce the influence of model errors on the calculation results (Fig. 3a). The length, width, and height of the CFD calculation domain are 13 km, 11 km, and 2 km, respectively, among which, nearly 2/3 of the buildings are distributed in the range of 10 - 40 meters, with the average height of the buildings of 32 m. The highest building in the area is 390 m, and the lowest building is 6 m.

The geometric model is divided by polyhedral mesh (Figs. 3c). The polyhedral mesh has much fewer cells than traditional tetrahedral mesh, but it doesn't affect the accuracy of calculation. Under the same number of grid cells, the numerical simulation results of polyhedral grids are more consistent with experimental data than tetrahedral grids (Zhang et al., 2020). When splitting the grid, the grids on the ground and near the building are much denser (Fig. 3b) (the minimum resolution is about 1 m), so that the influence of the building on the flow patterns can be described more finely. In the end, the number of unit grids generated is 382181, and the number of nodes is 1990224.

https://doi.org/10.5194/acp-2021-725
Preprint. Discussion started: 3 September 2021
© Author(s) 2021. CC BY 4.0 License.

Atmospheric Chemistry and Physics Discussions

2.3.2 Physical model and boundary conditions

In order to save computing resources, the RANS turbulence model with realizable k-ε is used in this study (Li et al., 2019; Li et al., 2006; Lei et al., 2004). The governing equations (1-3) of CFD are as follows:

$$\frac{\partial \overline{u_i}}{\partial t}+\overline{u_j}\frac{\partial \overline{u_i}}{\partial x_j}=-\frac{1}{\rho}\frac{\partial \overline{p}}{\partial x_i}+\frac{\mu}{\rho}\frac{\partial^2 \overline{u_i}}{\partial x_i x_j}-\frac{\partial}{\partial x_j}\left(\overline{u_i' u_j'}\right)+f_i, \quad (1)$$

$$\frac{\partial \overline{u_i}}{\partial x_j}=0 \ , \quad (2)$$

$$\frac{\partial \overline{T}}{\partial t}+\overline{u_i}\frac{\partial \overline{T}}{\partial x_i}=k\frac{\partial^2 \overline{T}}{\partial x_i^{2\prime}}, \quad (3)$$

where $\overline{u_i}$ and $\overline{u_j}$ mean the average velocity in west-east and south-north directions, respectively; u_i' and u_j' mean the turbulent variation; ρ means the air density; f_i means the buoyancy; and $\overline{T}$ means the mean temperature.

The ground and building surfaces are set to be no-slip, and the distribution of fluid velocity and pressure near the ground and the building surface is described by the blended wall function. The initial and boundary conditions (including velocity and temperature) of the calculation domain are obtained from the WRF grid closest to the CFD domain. Since the variables obtained by WRF simulation have a relatively large

https://doi.org/10.5194/acp-2021-725
Preprint. Discussion started: 3 September 2021
© Author(s) 2021. CC BY 4.0 License.

Atmospheric Chemistry and Physics Discussions

resolution of 1 km, the velocity components (U, V and W) and the temperature are interpolated to the boundary of CFD domain using the spline interpolation method and the linear interpolation method, respectively. For the turbulence intensity and turbulence viscosity ratio, the lateral and upper boundaries were set as constants with values of 0.1 and 10, respectively. The simulation time is from 0:00 BJT on 1 January 2019 to 23:00 BJT on 31 January 2019 and the simulation results are saved every 1 hour.

2.4 FLEXPART configuration

The FLEXPART model is a gas mass trajectory-particle diffusion model based on the Lagrange method developed by the Norwegian Atmospheric Research Institute. This study uses wind field data obtained from CFD model in combination with other meteorological data from WRF model to drive the FLEXPART. The simulation area is set to sub-domain B in Figure 3, with a horizontal grid resolution of 10 m × 10 m. The simulation time is from January 1, 2019 at 1:00 BJT to January 30, 2019 at 23:00 BJT. The time step of FLEXPART is 1 s, and the output time interval is 120 s. For the backward trajectory simulation, the turbulence option and the CBL turbulence parameterization scheme are turned off, since the turbulence is already resolved during the CFD simulation. Through backward trajectory simulation, the impact of traffic

https://doi.org/10.5194/acp-2021-725
Preprint. Discussion started: 3 September 2021
© Author(s) 2021. CC BY 4.0 License.

Atmospheric Chemistry and Physics Discussions

source on the receptor sites in the region can be effectively analyzed. Due to the high number of grids in the region and the fact that increasing the number of released particles leads to consuming more computational resources, the particle residence time is set as 2 h, and 2 tracer particles are released per hour at receptor sites in the course of simulation.

2.5 Meteorological observation data

Hourly near-surface meteorological observations from the Bank School City monitoring site (hereinafter referred as the BSC monitoring site), including 2 m temperature (T), 2 m relative humidity (RH), surface pressure (P), and 10 m wind speed (WS) in January 2019 are used to evaluate the WRF and CFD model results, with the statistical indexes including Pearson's correlation coefficient (R), root mean square error (RMSE), mean deviation (MB) and mean error (ME). The location of the BSC monitoring site (34.802375N, 113.675237E) is shown in Figure 3.

3. Results and discussions

3.1 Model evaluation

The performance of WRF model to simulate meteorological elements is an important basis for CFD and FLEXPART simulations. The hourly meteorological data

https://doi.org/10.5194/acp-2021-725
Preprint. Discussion started: 3 September 2021
© Author(s) 2021. CC BY 4.0 License.

Atmospheric Chemistry and Physics Discussions

for January 2019 obtained from the innermost nested simulation of the WRF model is selected to compare with observation data to verify the WRF model. Table 2 lists the statistical results of T, RH, P, and WS. The T and RH are slightly overestimated, with the MB values as 1.86 k and 5.95%, respectively, and the P and W are underestimated by the WRF model, with the MB values as 3.66 hpa and 1.44 m s^{-1}, respectively. The R values for T, RH and P are 0.80, 0.70 and 0.98, respectively, passed the 99% significance test, indicating that the variation characteristics of T, RH and P are well reproduced by the WRF model. WS is generally overestimated by WRF model (Temimi et al., 2020; He et al., 2014), which is also found in the present study with the RMSE of 1.97 m s^{-1}. The performance of the near-surface meteorology obtained by the WRF simulation is equivalent to previous studies (He et al., 2017b; Carvalho et al., 2012). In general, the temporal and spatial variability characteristics of the meteorological field in the area can be well simulated by the WRF model.

Since the time-varying boundary conditions in the calculation domain of CFD model are obtained from WRF model, the simulation performance of WRF model has an important influence on the CFD simulation results. The wind has an important influence on the transport and diffusion of air pollutants in the area (Zhang et al., 2015). Figure 4 shows the hourly wind observations and simulations at the BSC monitoring site in

https://doi.org/10.5194/acp-2021-725
Preprint. Discussion started: 3 September 2021
© Author(s) 2021. CC BY 4.0 License.

Atmospheric Chemistry and Physics Discussions

January 2019. Both WRF and CFD overestimate the wind speed to certain degrees (Fig. 4a). The average of observed wind speed is 0.92 m s^{-1}, with the value simulated by WRF and by CFD is 2.37 m s^{-1} and 2.00 m s^{-1}, respectively. The R values of WRF and CFD are 0.45 and 0.67, respectively, and passed the 99% significance test, demonstrating the refined CFD wind simulations is superior to that of the WRF. This might be due to the fact that the resolution of WRF simulation is not fine enough and the underlying surface is processed in a parameterized way that can't accurately describe the urban surface roughness. For the CFD model, the geometric model is used for the underlying surface, which could better reflect the urban surface conditions compared to parametric methods, but some urban layout settings (such as greenery) are missing in the construction of the geometric model. Figure 4b shows the comparison results of the observed and CFD simulated wind directions. It can be seen that the change of the wind direction is captured by CFD model well.

In general, WRF-CFD model simulation has good performance. After interpolation processing, they can provide more accurate and refined meteorological fields for FLEXPART model.

https://doi.org/10.5194/acp-2021-725
Preprint. Discussion started: 3 September 2021
© Author(s) 2021. CC BY 4.0 License.

Atmospheric Chemistry and Physics Discussions

3.2 The characteristics of the street-level wind fields

In urban areas, the complex spatial structure and layout of buildings have a great influence on the street-level wind field (Liu et al., 2018; Park et al., 2015), which is a crucial meteorological factor that controls the transport and diffusion of air pollutants. The street-level wind field characteristics were simulated by the S-TRACK and discussed comprehensively in this paper for the overall average in January as well as for different background wind directions, i.e., north, south, west and east, respectively.

3.2.1 The average wind field characteristics

Figures 5a-b illustrate the distribution of the average wind streamlines in January at the height of 5 m and 40 m, respectively. At the height of 5 m, the wind field structure is more complicated (Fig. 5a) than that at 40 m (Fig. 5b). The wind speed is relatively larger in the areas where the buildings are sparse and smaller. In addition, the flow fields diverge or converge due to the layout of buildings and streets, causing the wind direction inside blocks differ from the background wind direction greatly. At the height of 40 m (Fig. 5b), the influence of buildings on the wind field is diminished, which is mainly reflected by the fact that the wind directions at this height are more consistent to the background wind direction, consisting with previous studies (Sui et al., 2016).

https://doi.org/10.5194/acp-2021-725
Preprint. Discussion started: 3 September 2021
© Author(s) 2021. CC BY 4.0 License.

Atmospheric Chemistry and Physics Discussions

To clearly show the details of the wind field, a sub-domain A (Fig. 3a) with complex building structures is selected from the entire computational domain. The near-surface winds disperse or converge horizontally and climb or fall vertically with the building (Fig. 5c). During the climb or fall with the building, downwash winds with high wind speeds occurred (as shown in the red dashed circles). Due to the complexity of the building layout, local circulation is formed on the west side of the BSC monitoring site, making the airflow around the building on the south side of the station pile up and form an obvious convergence area (Fig. 5d), which is not conducive to the air circulation and pollution diffusion (as shown in the red box).

3.2.2 The wind field characteristics under different background wind directions

Figure 6 shows the distributions of near-surface wind and its divergence under four different background wind directions. In general, the overall wind direction in the area is consistent with the background wind direction, but the airflow near-surface is significantly affected by the building layout and thus formed local circulations with dispersion and convergence zones. The wind speeds in the areas with dense buildings are significantly smaller than those in open areas (Figs. 6a-1, 6b-1, 6c-1, and 6d-1), which is attributed to the obvious frictional dragging effect of the dense buildings. The overall

https://doi.org/10.5194/acp-2021-725
Preprint. Discussion started: 3 September 2021
© Author(s) 2021. CC BY 4.0 License.

Atmospheric Chemistry and Physics Discussions

wind direction of the area is generally the same as the background wind direction, but the airflow is dispersed or converged by the influence of the building layout, resulting in a great difference between the wind direction inside the block and the background wind direction. When the background wind direction is north or west (Figs. 6b and 6c), the overall wind speed in the area is relatively large. This is mainly due to the temperate monsoon climate in Zhengzhou, where northwest and west winds prevail in winter and wind speeds are relatively high. The wind speed inside the block is smaller than the background wind speed, which is attributed to the obvious frictional dragging effect of the dense buildings on the flow field.

The windward side of the building is mostly a divergence zone and the leeward side is mainly a convergence zone, which is more obvious for higher buildings. When the airflow meets the building, the airflow on the windward side of the building is blocked and thus spreads outward, forming a dispersion zone; while the airflow on the leeward side of the building converges and generates a vortex with lower wind speed, forming a convergence zone. Take the building where the BSC monitoring site is located as an example, when the background wind direction is west, the wind speed on the windward side of the building is higher and diffused outward by the building blockage (Fig. 6c-2), resulting in a significant divergence zone (Fig. 6c-3). It can be seen that the ventilation is

https://doi.org/10.5194/acp-2021-725
Preprint. Discussion started: 3 September 2021
© Author(s) 2021. CC BY 4.0 License.

Atmospheric Chemistry and Physics Discussions

better when the dominant airflow is in the same direction as building layout (Fig. 6c). In the process of urban construction, the influence of prevailing wind direction on the layout of buildings should be considered, which could effectively improve the efficiency of urban ventilation.

3.3 Potential impact of a traffic source

In this section, the S-TRACK system is used to analyze potential impact of a main traffic road in sub-domain B (Fig. 3a) on several receptor sites nearby with different heights and locations. January 2019 was selected as the simulation period. The sub-domain B includes a number of schools and residential areas. Additionally, potential impact of traffic source under different background wind directions was explored. The residence-time analysis (RTA), which has been previously used to identify the accounted contribution of emission sources to air quality of receptors (Yu, 2017; Salvador et al., 2008; Hopke et al., 2005; Poirot et al., 2001; Ashbaugh et al., 1985), was selected in this study to assess the potential contribution ratio of the traffic source on receptors. The RTA is expressed as:

$$R_{i,j} = \frac{\tau_{i,j}}{t} \quad (4)$$

https://doi.org/10.5194/acp-2021-725
Preprint. Discussion started: 3 September 2021
© Author(s) 2021. CC BY 4.0 License.

Atmospheric Chemistry and Physics Discussions

where $R_{i,j}$ indicates the contribution ratio of the grid (i,j) to receptor; $\tau_{i,j}$ means the residence time in the grid (i,j) and t means the total residence time in all grids.

3.3.1 Potential impact of traffic source at different sites in winter

In order to analyze the potential impact of the traffic source on different locations, the receptor sites were selected at different locations and heights as listed in Table 3. For the receptor site S1, which is about 400 m from the traffic road, located in a dense building area with the building height at 30 to 40 meters, the potential contribution ratio of the traffic source on the receptor site was calculated to be 1.81%. For the receptor site S2, which is about 300 m from the traffic road, located in an open area and surrounded by low buildings, the potential contribution ratio of the traffic source is determined to be 2.38%. It might be inferred that the wind field difference partially resulted from the influence of buildings layout leads to the higher contribution rate to S2. Additionally, the difference in the wind environment at different locations might be another influence factor for the difference.

Receptor sites S2-S8 are selected to investigate differences in contributions of traffic source to receptor sites at different heights. The potential contribution ratios of the road are 2.38%, 2.57%, 2.71%, and 2.98% for receptor sites S2 to S5, with the height of

https://doi.org/10.5194/acp-2021-725
Preprint. Discussion started: 3 September 2021
© Author(s) 2021. CC BY 4.0 License.

Atmospheric Chemistry and Physics Discussions

2 m, 5 m, 10 m, and 15 m, respectively (Table 3). However, as the receptor height continues to rise, namely from S5 to S8, the potential contribution ratio of the road gradually decreases from 2.98% to 1.94%. The potential impact of the traffic source is the greatest when the receptor site is located at a height of 15 m, suggesting the air quality at that height is most susceptible to traffic emissions when the building is approximately 400 meters from traffic road. In addition, from density distribution of all trajectory points that have passed through the traffic road (Figs. 7), it can be seen that the road section with lager potential impact to air pollution at receptor sites is both located to their northeast, which might be a result of the combination effect of the background wind field and the building layout.

3.3.2 Potential impact of traffic source under different background wind directions

In order to investigate the potential impact of traffic source under different background wind directions, the receptor site S2 under the east, the south, the west, and the north wind directions was classified from the simulation period (not shown). The potential contribution ratios of traffic source were calculated to be 2.45%, 0.07%, 1.98%, and 2.97% for the east, the south, the west, and the north wind directions, respectively, revealing that the difference in potential impact is largest between the south and north

https://doi.org/10.5194/acp-2021-725
Preprint. Discussion started: 3 September 2021
© Author(s) 2021. CC BY 4.0 License.


wind directions. When the background wind direction is south, the receptor site is located upwind of the road, and the road traffic source contributes very little to the receptor site. On the contrary, the receptor site is downwind of the road when the wind direction is north, and the contribution ratio of road traffic source to the receptor site is the greatest. When the background wind direction is east and west, the contribution ratio to the receptor point is similar and lies between the ratios that under south and north wind directions. The higher contribution ratio during westerly winds relatively to that under easterly winds may partially due to the denser distribution of buildings upwind of the receptor site. The results of the potential impact of traffic source under different background wind conditions is helpful to understand the streel-level pollution transport characteristics and provide effective suggestions for the pollution control.

4. Conclusions

A street-level pollutant tracking system was developed to simulate micro-scale meteorology and used to analyze the characteristics of wind environment and the potential traffic source contribution of air pollution to receptors through backward simulations in a city district. In general, the S-TRACK system is effective in simulating the street-level meteorological and pollution problems. The presence of buildings has a

https://doi.org/10.5194/acp-2021-725
Preprint. Discussion started: 3 September 2021
© Author(s) 2021. CC BY 4.0 License.

Atmospheric Chemistry and Physics Discussions

significant effect on the wind environment, i.e., the dragging effect of dense buildings renders the wind speed inside the block smaller than the background wind speed. The ventilation is better when the dominant airflow is consistent with the direction of building layout. Influenced by the building layout, the airflow near-surface is formed with divergence and convergence zones. The windward side of the building is mostly a divergence zone and the leeward side is mostly a convergence zone, which is more obvious for higher buildings.

As a test case, the S-TRACK system has been used to investigate the potential impact of a traffic source on receptor sites with different locations, heights and background wind directions. The method of RTA was used to assess the potential impact of traffic sources on receptor air quality. The potential impact of traffic sources on a specific receptor site varies under different background wind directions, which were estimated to be 2.45%, 0.07%, 1.98%, and 2.97% for the east, the south, the west, and the north wind directions, respectively. For a specific location of this case study, the potential traffic contribution ratios also varied with height at about 2.38%, 2.57%, 2.71%, 2.98%, 2.75%, 2.30% and 1.94% at 2, 5, 10, 15, 20, 40, 50 m, respectively, manifesting a significant trend of increasing and then decreasing with height.

https://doi.org/10.5194/acp-2021-725
Preprint. Discussion started: 3 September 2021
© Author(s) 2021. CC BY 4.0 License.

Atmospheric Chemistry and Physics Discussions

In the future, more simulation experiments with different building layouts, wind field environments, and distances between traffic source and receptor are required to study the potential impact of street-level pollution sources in-depth. In addition, due to the unavailability of street-level emissions in the Jinshui district, further quantitative impact analysis of traffic sources could not be conducted in this study. Future in-depth investigations of the relationship between meteorological conditions, buildings and various emissions (point, area and line sources) in the street-level are also needed as a better theoretical basis and practical suggestions for effective management of regional pollution in a city.

Code/data availability

All source code and data can be accessed by contacting the corresponding authors Sunling Gong (gongsl@cma.gov.cn) and Lei Zhang (leiz09@cma.gov.cn).

Authors contribution

Sunling Gong and Lei Zhang designed the research. Huan Zhang performed the simulations and wrote the manuscript with suggestions from all authors. Jingyue Mo, Huabing Ke, and Shuhua Lu assisted with data processing. Jianjun He, Yaqiang Wang

https://doi.org/10.5194/acp-2021-725
Preprint. Discussion started: 3 September 2021
© Author(s) 2021. CC BY 4.0 License.

Atmospheric Chemistry and Physics Discussions

and Lixin Shi participated in the scientific interpretation and discussion. All authors contributed to the discussion and improvement of the manuscript.

Competing interests

The authors declare that they have no conflict of interest.

Acknowledgments

The authors would like to acknowledge Bin Cui and Lin Zhang from Peking University and Liangfu Chen from Chinese Academy of Sciences for their valuable suggestions to improve the article.

https://doi.org/10.5194/acp-2021-725
Preprint. Discussion started: 3 September 2021
© Author(s) 2021. CC BY 4.0 License.

Atmospheric Chemistry and Physics Discussions

References

Ashbaugh, L., Malm, W., and Sadeh, W.: A residence time probability analysis of sulfur concentrations at grand Canyon national park, Atmos. Environ., 19, 1263-1270, https://doi.org/10.1016/0004-6981(85)90256-2, 1985.

Aynsley, R.: Politics of pedestrian level urban wind control, Build Environ, 24, 291-295, https://doi.org/10.1016/0360-1323(89)90022-X, 1989.

Brioude, J., Arnold, D., Stohl, A., Cassiani, M., Morton, D., Seibert, P., Angevine, W., Evan, S., Dingwell, A., Fast, J. D., Easter, R. C., Pisso, I., Burkhart, J., and Wotawa, G.: The Lagrangian particle dispersion model FLEXPART-WRF version 3.1, Geosci. Model Dev. (GMD), 6, 1889-1904, https://doi.org/10.5194/gmd-6-1889-2013, 2013.

Carvalho, D., Rocha, A., Gómez-Gesteira, M., and Santos, C.: A sensitivity study of the WRF model in wind simulation for an area of high wind energy, Environ. Model. Software, 33, 23-34, https://doi.org/10.1016/j.envsoft.2012.01.019, 2012.

Cécé, R., Bernard, D., Brioude, J., and Zahibo, N.: Microscale anthropogenic pollution modelling in a small tropical island during weak trade winds: Lagrangian particle dispersion simulations using real nested LES meteorological fields, Atmos. Environ., 139, 98-112, https://doi.org/10.1016/j.atmosenv.2016.05.028, 2016.

Chen, F. and Dudhia, J.: Coupling an Advanced Land Surface–Hydrology Model with the Penn State–NCAR MM5 Modeling System. Part I: Model Implementation and Sensitivity, Mon. Weather Rev., 129, 569-585, https://doi.org/10.1175/1520-0493(2001)129<0569:CAALSH>2.0.CO;2, 2001.

de Foy, B., Burton, S. P., Ferrare, R. A., Hostetler, C. A., Hair, J. W., Wiedinmyer, C., and Molina, L. T.: Aerosol plume transport and transformation in high spectral resolution lidar measurements and WRF-Flexpart simulations during the MILAGRO Field Campaign, Atmos. Chem. Phys., 11, 3543-3563, https://doi.org/10.5194/acp-11-3543-2011, 2011.

Ehrhard, J., Khatib, I., Winkler, C., Kunz, R., Moussiopoulos, N., and Ernst, G.: The microscale model MIMO: development and assessment, J. Wind. Eng. Ind. Aerodyn., 85, 163-176, https://doi.org/10.1016/S0167-6105(99)00137-3, 2000.

Fast, J. D. and Easter, R. C.: A Lagrangian particle dispersion model compatible with WRF, 7th WRF Users Workshop, NCAR, 19–22, 2006.

Fernando, H., Zajic, D., Sabatino, S. D., Dimitrova, R., and Dallman, A.: Flow, turbulence, and pollutant dispersion in urban atmosphere, Phys. Fluids, 22, 051301, https://doi.org/10.1063/1.3407662, 2010.

Gao, Y., Shan, H., Zhang, S., Sheng, L., Li, J., Zhang, J., Ma, M., Meng, H., Luo, K., Gao, H., and Yao, X.: Characteristics and sources of PM2.5 with focus on two severe pollution events in a coastal city of Qingdao, China, Chemosphere, 247, 125861, https://doi.org/10.1016/j.chemosphere.2020.125861, 2020.

Gosman, A. D.: Developments in CFD for industrial and environmental applications in wind engineering, J. Wind. Eng. Ind. Aerodyn., 81, 21-39, https://doi.org/10.1016/S0167-6105(99)00007-0, 1999.

He, J., Mao, H., Gong, S., Yu, Y., and Zou, C.: Investigation of particulate matter regional transport in Beijing based on numerical simulation, Aerosol Air Qual. Res., 17, 1181-1189, https://doi.org/10.4209/AAQR.2016.03.0110, 2017a.

He, J., Zhang, L., Yao, Z., Che, H., Gong, S., Wang, M., Zhao, M., and Jing, B.: Source apportionment of particulate matter based on numerical simulation during a severe pollution period in Tangshan, North China, Environ. Pollut., 266, 115133, https://doi.org/10.1016/j.envpol.2020.115133, 2020.

He, J. J., Yu, Y., Liu, N., Zhao, S. P., and Chen, J. B.: Impact of land surface information on WRFs performance in complex terrain area, Chin. J. Atmos. Sci., 38, 484-498, https://doi.org/10.3878/j.issn.1006-9895.2013, 2014.

He, J. J., Yu, Y., Yu, L. J., Liu, N., and Zhao, S. P.: Impacts of uncertainty in land surface information on simulated surface temperature and precipitation over China, Int J Climatol, 37, 829-847, https://doi.org/10.1002/joc.5041, 2017b.

https://doi.org/10.5194/acp-2021-725
Preprint. Discussion started: 3 September 2021
© Author(s) 2021. CC BY 4.0 License.

Atmospheric Chemistry and Physics Discussions

Hendricks, E. A., Diehl, S. R., Burrows, D. A., and Keith, R.: Evaluation of a Fast-Running Urban Dispersion Modeling System Using Joint Urban 2003 Field Data, J Appl Meteorol Climatol, 46, 2165-2179, https://doi.org/10.1175/2006JAMC1289.1, 2007.

Heo, J., Foy, B. D., Olson, M. R., Pakbin, P., Sioutas, C., and Schauer, J.: Impact of regional transport on the anthropogenic and biogenic secondary organic aerosols in the Los Angeles Basin, Atmos. Environ., 103, 171-179, https://doi.org/10.1016/J.ATMOSENV.2014.12.041, 2015.

Hopke, P., Zhou, L., and Poirot, R.: Reconciling trajectory ensemble receptor model results with emissions, Environ. Sci. Technol., 39(20), 7980-7983, https://doi.org/10.1021/es049816g, 2005.

Iacono, M. J., Delamere, J. S., Mlawer, E. J., Shephard, M. W., and Collins, W. D.: Radiative Forcing by Long-Lived Greenhouse Gases: Calculations with the AER Radiative Transfer Models, J. Geophys. Res.-Atmos., 113, D13103, https://doi.org/10.1029/2008JD009944, 2008.

Kurppa, M., Hellsten, A., Auvinen, M., Raasch, S., Vesala, T., and Järvi, L.: Ventilation and Air Quality in City Blocks Using Large-Eddy SimulatioŽ Urban Planning Perspective, Atmosphere, 9, 65, https://doi.org/10.3390/ATMOS9020065, 2018.

Kwak, K.-H., Baik, J.-J., Ryu, Y.-H., and Lee, S.-H.: Urban air quality simulation in a high-rise building area using a CFD model coupled with mesoscale meteorological and chemistry-transport models, Atmos. Environ., 100, 167-177, https://doi.org/10.1016/j.atmosenv.2014.10.059, 2015.

Lei, L., Fei, H., Cheng, X. L., and Han, H. Y.: The application of computational fluid dynamics to pedestrian level wind safety problem induced by high-rise buildings, Chin. Phys. B, 13, 1070-1075, https://doi.org/10.1088/1009-1963/13/7/018, 2004.

Lei, L. I., Yang, L., Zhang, L. J., and Jiang, Y.: Numerical Study on the Impact of Ground Heating and Ambient Wind Speed on Flow Fields in Street Canyons, Adv Atmos Sci, 29, 1227-1237, https://doi.org/10.1007/s00376-012-1066-3, 2012.

Li, L., Hu, F., Cheng, X. L., Jiang, J. H., and Ma, X. G.: Numerical simulation of the flow within and over an intersection model with Reynolds-averaged Navier-Stokes method, Chin. Phys. B, 15, 149-155, https://doi.org/10.1088/1009-1963/15/1/024, 2006.

Li, S., Sun, X., Zhang, S., Zhao, S., and Zhang, R.: A Study on Microscale Wind Simulations with a Coupled WRF–CFD Model in the Chongli Mountain Region of Hebei Province, China, Atmosphere, 10, 731, https://doi.org/10.3390/atmos10120731, 2019.

Li, X.-X., Liu, C.-H., and Leung, D. Y. C.: Large-Eddy Simulation of Flow and Pollutant Dispersion in High-Aspect-Ratio Urban Street Canyons with Wall Model, Bound. Layer Meteor., 129, 249-268, https://doi.org/10.1007/s10546-008-9313-y, 2008.

Lin, Y. L., Farley, R. D., and Orville, H. D.: Bulk Parameterization of the Snow Field in a Cloud Model, J APPL METEOROL, 22, 1065-1092, https://doi.org/10.1175/1520-0450(1983)022<1065:BPOTSF>2.0.CO;2, 1983.

Liu, N., Yu, Y., He, J., and Zhao, S.: Integrated modeling of urban-scale pollutant transport: application in a semi-arid urban valley, Northwestern China (SCI), Atmospheric Pollut. Res., 4, 306-314, https://doi.org/10.5094/APR.2013.034, 2013.

Liu, S., Pan, W., Zhao, X., Zhang, H., Cheng, X., Long, Z., and Chen, Q.: Influence of surrounding buildings on wind flow around a building predicted by CFD simulations, Build Environ, 140, 1-10, https://doi.org/10.1016/j.buildenv.2018.05.011, 2018.

Macdonald, R. W., Griffiths, R. F., and Cheah, S. C.: Field experiments of dispersion through regular arrays of cubic structures, Atmos. Environ., 31, 783-795, https://doi.org/10.1016/S1352-2310(96)00263-4, 1997.

Madala, S., Satyanarayana, A. N., Srinivas, C., and Kumar, M.: Mesoscale atmospheric flow-field simulations for air quality modeling over complex terrain region of Ranchi in eastern India using WRF, Atmos. Environ., 107, 315-328, https://doi.org/10.1016/J.ATMOSENV.2015.02.059, 2015.

https://doi.org/10.5194/acp-2021-725
Preprint. Discussion started: 3 September 2021
© Author(s) 2021. CC BY 4.0 License.

Atmospheric Chemistry and Physics Discussions

Mavroidis, I., Rf., G., and Dj., H.: Field and wind tunnel investigations of plume dispersion around single surface obstacles, Atmos. Environ., 37, 2903-2918, https://doi.org/10.1016/S1352-2310(03)00300-5, 2003.

Milliez, M. and Carissimo, B.: Computational Fluid Dynamical Modelling of Concentration Fluctuations in an Idealized Urban Area, Bound. Layer Meteor., 127, 241-259, https://doi.org/10.1007/s10546-008-9266-1, 2008.

Nakanishi, M. and Niino, H.: An Improved Mellor–Yamada Level-3 Model: Its Numerical Stability and Application to a Regional Prediction of Advection Fog, Bound. Layer Meteor., 119, 397-407, https://doi.org/10.1007/S10546-005-9030-8, 2006.

Nelson, M. A., Brown, M. J., Halverson, S. A., Bieringer, P. E., Annunzio, A., Bieberbach, G., and Meech, S.: A Case Study of the Weather Research and Forecasting Model Applied to the Joint Urban 2003 Tracer Field Experiment. Part 2: Gas Tracer Dispersion, Bound. Layer Meteor., 161, 461-490, https://doi.org/10.1007/s10546-016-0188-z, 2016.

Park, S. B., Baik, J. J., and Han, B. S.: Large-eddy simulation of turbulent flow in a densely built-up urban area, Environ. Fluid Mech., 15, 235-250, https://doi.org/10.1007/s10652-013-9306-3, 2015.

Poirot, R., Wishinski, P., Hopke, P., and Polissar, A.: Comparative application of multiple receptor methods to identify aerosol sources in northern Vermont, Environ. Sci. Technol., 35(23), 4622-4636, https://doi.org/10.1021/es011442t, 2001.

Sada, K. and Sato, A.: Numerical calculation of flow and stack-gas concentration fluctuation around a cubical building, Atmos. Environ., 36, 5527-5534, https://doi.org/10.1016/S1352-2310(02)00668-4, 2002.

Salvador, P., Artíñano, B., Querol, X., and Alastuey, A.: A combined analysis of backward trajectories and aerosol chemistry to characterise long-range transport episodes of particulate matter: the madrid air basin, a case study, Sci. Total Environ., 390(2-3), 495-506, https://doi.org/10.1016/j.scitotenv.2007.10.052, 2008.

Sandeepan, B., Rakesh, P. T., and Venkatesan, R.: Numerical simulation of observed submesoscale plume meandering under nocturnal drainage flow, Atmos. Environ., 69, 29-36, https://doi.org/10.1016/J.ATMOSENV.2012.12.007, 2013.

Stohl, A.: A backward modeling study of intercontinental pollution transport using aircraft measurements, J. Geophys. Res., 108, 4370, https://doi.org/10.1029/2002jd002862, 2003.

Stohl, A., Forster, C., Frank, A., Seibert, P., and Wotawa, G.: Technical note: The Lagrangian particle dispersion model FLEXPART version 6.2, Atmos. Chem. Phys., 5, 2461-2474, https://doi.org/10.5194/ACP-5-2461-2005, 2005.

Sui, L., Jiang, M., Li, Z., and Zhou, S.: Diffusion effect analysis of pollution gas under the impact of urban three-dimensional pattern, in:5th International Conference on Energy and Environmental Protection, Shengzhen, China, 17-18, September 2016, 903-909, 2016.

Temimi, M., Fonseca, R., Reddy, N. N., Weston, M., and Naqbi, H. A.: Assessing The Impact of Changes in Land Surface Conditions on WRF Predictions in Arid Regions, J Hydrometeorol, 21, 2829-2853, https://doi.org/10.1175/JHM-D-20-0083.1, 2020.

Tewari, M., Kusaka, H., Chen, F., Coirier, W. J., Kim, S., Wyszogrodzki, A. A., and Warner, T. T.: Impact of coupling a microscale computational fluid dynamics model with a mesoscale model on urban scale contaminant transport and dispersion, Atmos. Res., 96, 656-664, https://doi.org/10.1016/j.atmosres.2010.01.006, 2010.

W., S. J., Stoll，R., Gowardhan，A., A., K. K., and M., B. J.: One-Way Coupling of the WRF-QUIC Urban Dispersion Modeling System, J Appl Meteorol Climatol, 54, 2119-2139, https://doi.org/10.1175/JAMC-D-15-0020.1, 2015.

Yu, C., Zhao, T., Bai, Y., Zhang, L., Kong, S., Yu, X., He, J., Cui, C., Yang, J., You, Y., Ma, G., Wu, M., and Chang, J.: Heavy air pollution with a unique “non-stagnant” atmospheric boundary layer in the Yangtze River middle basin aggravated by regional transport of PM2.5 over China, Atmos. Chem. Phys., 20, 7217-7230, https://doi.org/10.5194/acp-20-7217-2020, 2020.

https://doi.org/10.5194/acp-2021-725
Preprint. Discussion started: 3 September 2021
© Author(s) 2021. CC BY 4.0 License.

Yu, T. Y.: Source identification of emission sources for hydrocarbon with backward trajectory model and statistical methods, Pol. J. Environ. Stud., 26(2), 893-902, https://doi.org/10.15244/pjoes/65744, 2017.

Yucong, M., Shuhua, L., Hui, Z., Yijia, Z., Bicheng, C., and Shu, W.: A multi-scale urban atmospheric dispersion model for emergency management, Adv Atmos Sci, 31, 1353-1365, https://doi.org/10.1007/s00376-014-3254-9, 2014.

Zhang, H., Xu, T., Zong, Y., Tang, H., Liu, X., and Wang, Y.: Influence of Meteorological Conditions on Pollutant Dispersion in Street Canyon, Procedia Engineering, 121, 899-905, https://doi.org/10.1016/J.PROENG.2015.09.047, 2015.

Zhang, H., Tang, S., Yue, H., Wu, K., Zhu, Y., Liu, C.-J., Liang, B., and Li, C.: Comparison of Computational Fluid Dynamic Simulation of a Stirred Tank with Polyhedral and Tetrahedral Meshes, Iran. J. Chem. Chem. Eng., 39, 311-319, https://doi.org/10.30492/IJCCE.2019.34950, 2020.

Zheng, Y., Miao, Y., Liu, S., Chen, B., Zheng, H., and Wang, S.: Simulating Flow and Dispersion by Using WRF-CFD Coupled Model in a Built-Up Area of Shenyang, China, Adv. Meteorol, 2015, 1-15, https://doi.org/10.1155/2015/528618, 2015.

https://doi.org/10.5194/acp-2021-725
Preprint. Discussion started: 3 September 2021
© Author(s) 2021. CC BY 4.0 License.

Atmospheric Chemistry and Physics Discussions

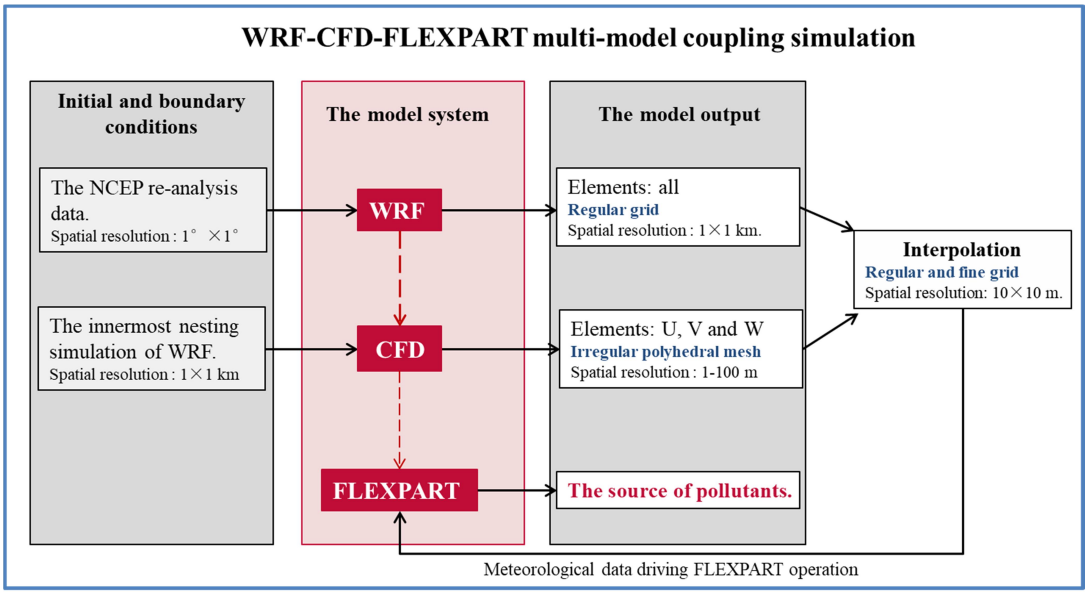

Figure 1: The S-TRACK system: The role of WRF, CFD and FLEXPART in the S-TRACK system and the process of gradual refinement of resolution.

535

https://doi.org/10.5194/acp-2021-725
Preprint. Discussion started: 3 September 2021
© Author(s) 2021. CC BY 4.0 License.

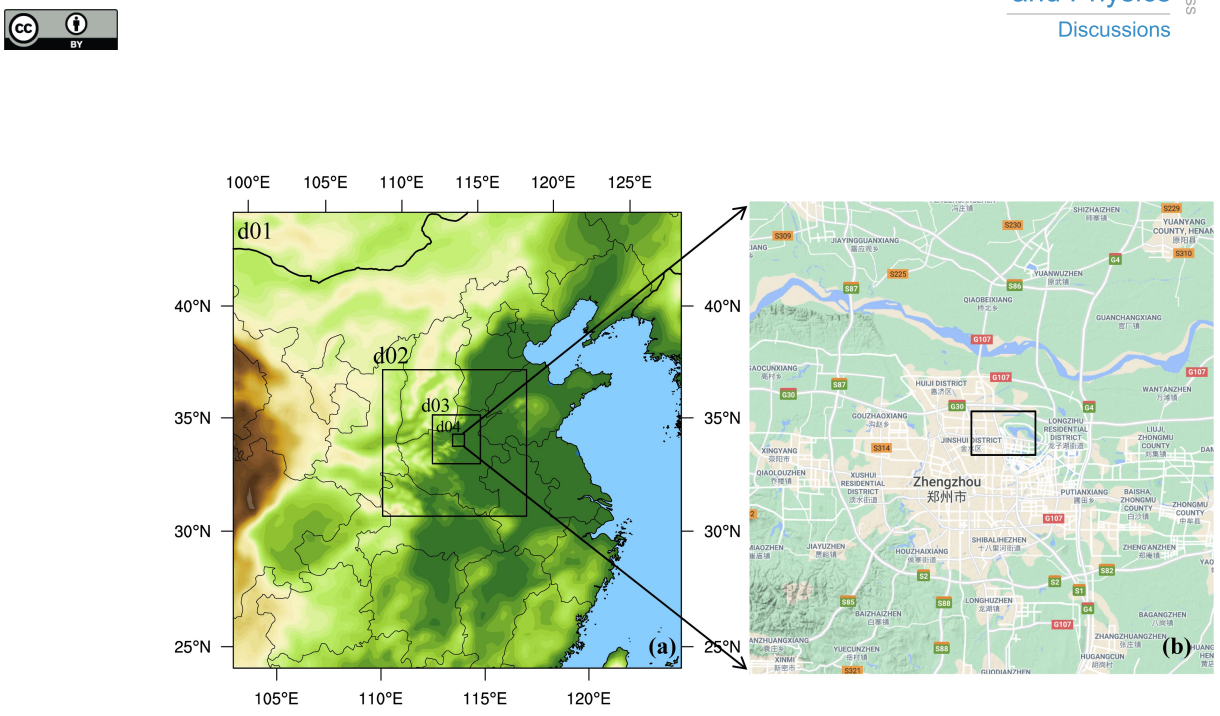

Figure 2: Domain configuration of the WRF model: (a) the range of the four nested domains (d1-d4); (b) the innermost nested domain (d4), within which the black box represents the CFD simulation domain (extracted from © Google Maps 2021).

540

https://doi.org/10.5194/acp-2021-725
Preprint. Discussion started: 3 September 2021
© Author(s) 2021. CC BY 4.0 License.

Atmospheric Chemistry and Physics Discussions

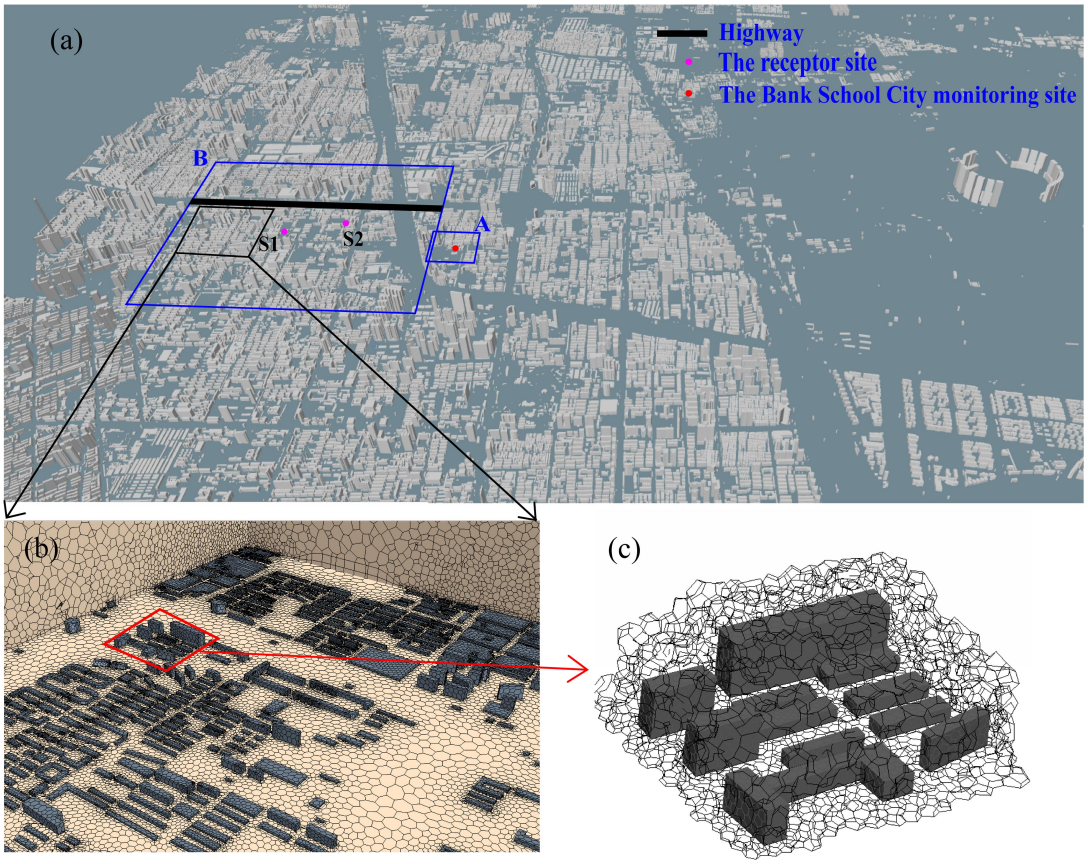

Figure 3: The computational domain of the CFD model is shown in (a). The sub-domain A is used for detailed analysis of the wind environment, and the Bank School City (BSC) monitoring site is marked with the red dot. Sub-domain B is used to analyze the potential impact of traffic source on receptor sites in the region, with magenta dots (S1 and S2) indicating the receptor sites and a black line indicating the highway. The polyhedral mesh is used to divide the CFD modeling area. The mesh details of the vertical cross section and building surface are shown in (b), and the 3D meshes are shown in (c).

https://doi.org/10.5194/acp-2021-725
Preprint. Discussion started: 3 September 2021
© Author(s) 2021. CC BY 4.0 License.

Atmospheric Chemistry and Physics Discussions

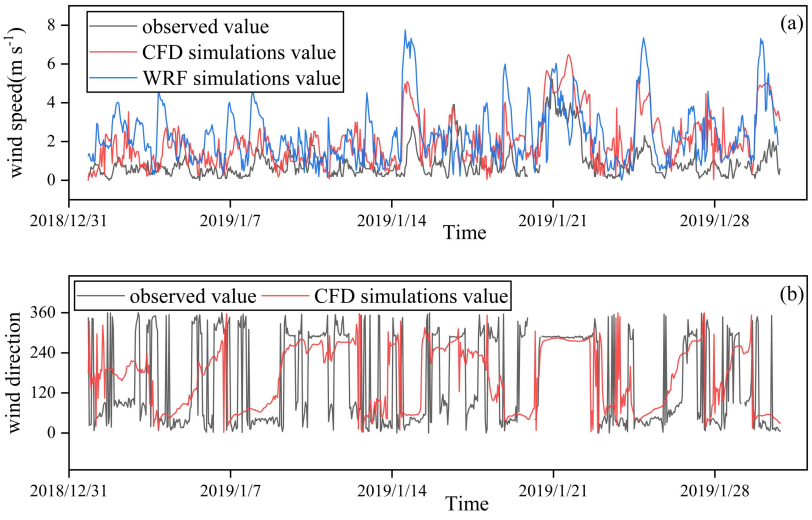

Figure 4: Evaluation of the wind simulation results at the BSC monitoring site (see in Fig. 3a): (a) the simulated, by WRF (blue line) and CFD (red line) model, respectively, and the observed (grey line) hourly near-surface wind speeds; (b) the simulated, by CFD (red line), and observed (grey line) hourly near-surface wind directions.

https://doi.org/10.5194/acp-2021-725
Preprint. Discussion started: 3 September 2021
© Author(s) 2021. CC BY 4.0 License.

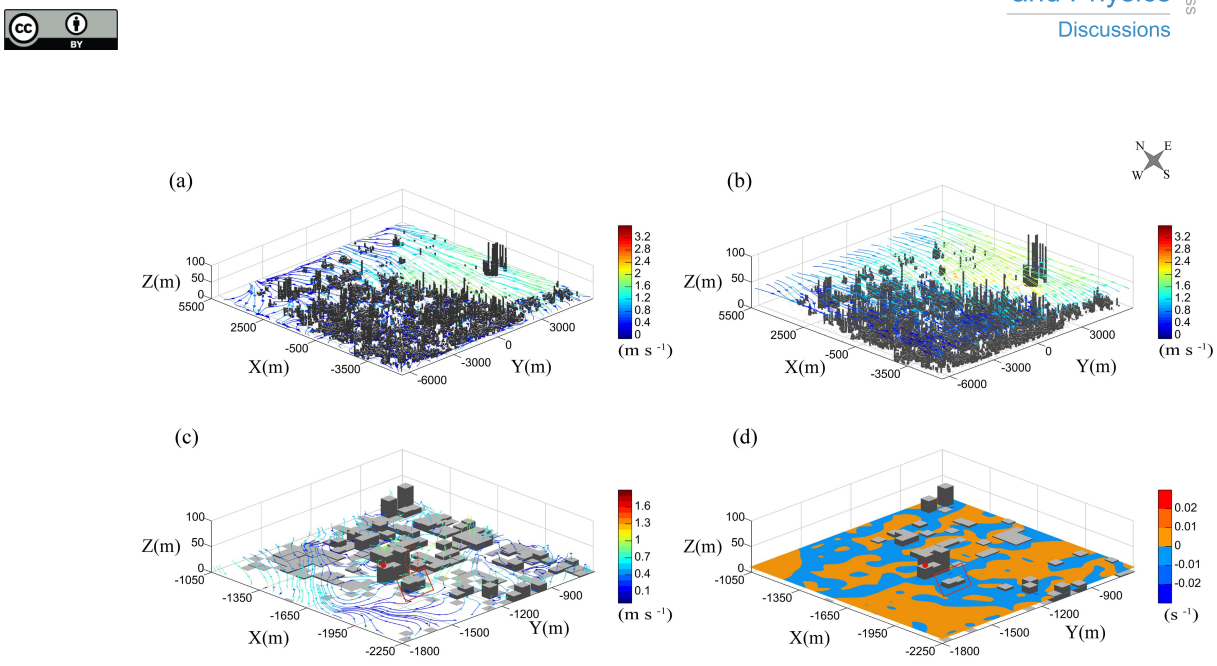

Figure 5: The simulated wind streamlines at the height of 5 m (a) and 40 m (b) averaged in January 2019 in the whole S-TRACK simulation domain; the simulated wind streamlines (c) and divergence (d) at the near-surface averaged in January 2019 in the sub-domain A (see in Fig. 3a).
560 **The BSC monitoring site is marked with red dot.**

https://doi.org/10.5194/acp-2021-725
Preprint. Discussion started: 3 September 2021
© Author(s) 2021. CC BY 4.0 License.

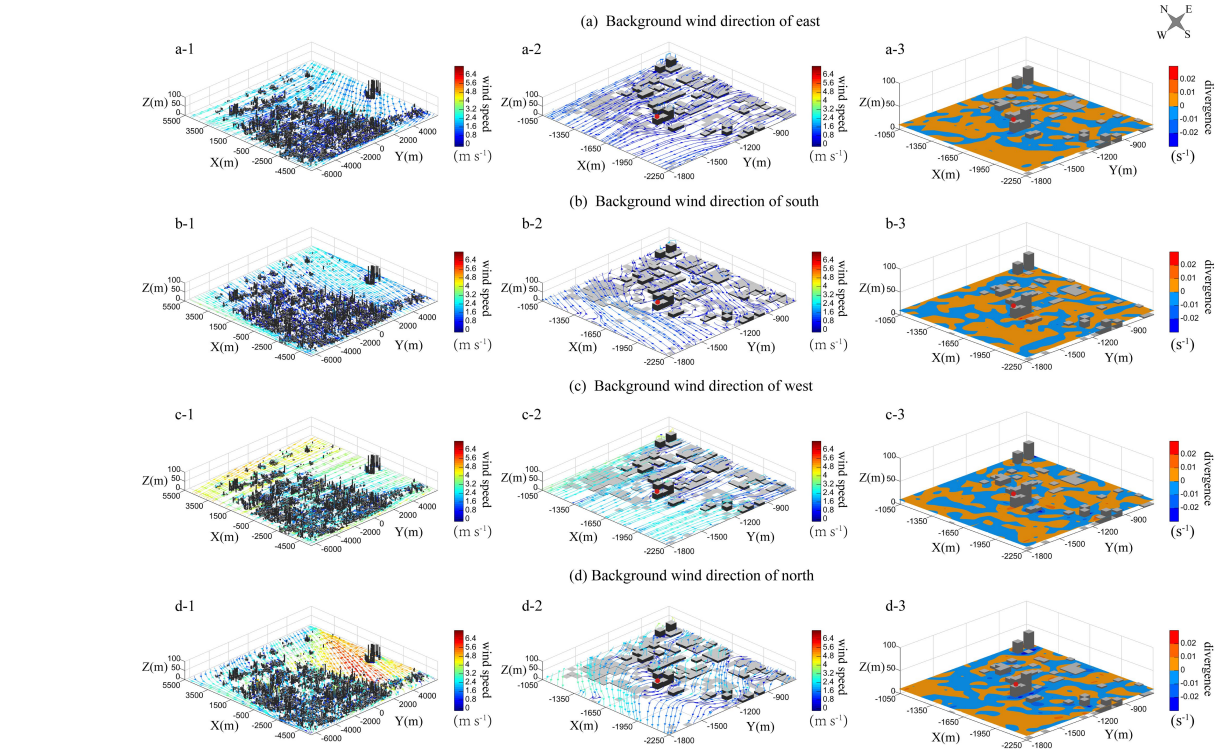

Figure 6: The wind field streamlines and divergences under the background wind directions of east (a), south (b), west (c) and north (d). The BSC monitoring site is marked with red dot.

565

https://doi.org/10.5194/acp-2021-725
Preprint. Discussion started: 3 September 2021
© Author(s) 2021. CC BY 4.0 License.

Atmospheric Chemistry and Physics Discussions

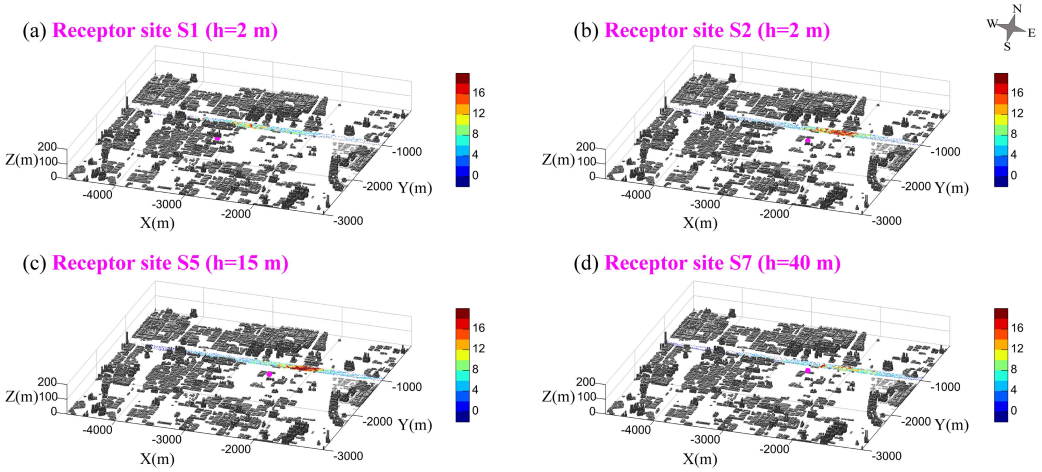

Figure 7: Density distribution of all trajectory points passing through the traffic road that released from different receptor sites (S1, S2, S5, and S7, see details in Table 3). The four receptor sites are all marked with magenta dots.

570

https://doi.org/10.5194/acp-2021-725
Preprint. Discussion started: 3 September 2021
© Author(s) 2021. CC BY 4.0 License.

Atmospheric Chemistry and Physics Discussions

Table 1 Parameterization scheme for the physical processes set up in the WRF model.

Physical management	Parameterization	Reference
Microphysics scheme	Lin	Lin et al. (1983)
Longwave radiation scheme	RRTMG	Iacono et al. (2008)
Shortwave radiation scheme	RRTMG	Iacono et al. (2008)
Land surface scheme	Noah	Chen and Dudhia (2001)
Planetary boundary layer scheme	MYNN3	Nakanishi and Niino (2006)

Table 2 Statistical performances of the hourly near-surface meteorologies simulated by the WRF model.

	R	MB	ME	RMSE
T	0.80	-1.86 (K)	2.33 (K)	2.82 (K)
RH	0.70	-5.95 (%)	11.5 (%)	15.0 (%)
P	0.98	3.66 (hpa)	3.66 (hpa)	3.77 (hpa)
WS	0.45	1.44 (m s^{-1})	1.58 (m s^{-1})	1.97 (m s^{-1})

575 **Table 3 Locations of receptor sites and potential contribution ratios of traffic sources.**

Receptor site	Location (x, y, z)	potential contribution ratio
S1	(-3200 m, -1420 m, 2 m)	1.81%
S2	(-2500 m, -1300 m, 2 m)	2.38%
S3	(-2500 m, -1300 m, 5 m)	2.57%
S4	(-2500 m, -1300 m, 10 m)	2.71%
S5	(-2500 m, -1300 m, 15 m)	2.98%
S6	(-2500 m, -1300 m, 20 m)	2.75%
S7	(-2500 m, -1300 m, 40 m)	2.30%
S8	(-2500 m, -1300 m, 50 m)	1.94%